Journal of Chromatography A, 1218 (2011) 5108–5114

Contents lists available at ScienceDirect

Journal of Chromatography A

journal homepage: www.elsevier.com/locate/chroma

The three-dimensional model for helical columns on type-J synchronous counter-current chromatography

Y.H. Guan [a,b,*], Remco van den Heuvel [a]

[a] Brunel Institute for Bioengineering, Brunel University West London, Uxbridge, Middlesex UB8 3PH, UK
[b] State Key Laboratory of Bioreactor Engineering, School of Biotechnology, East China University of Science & Technology, Shanghai 200237, China

ARTICLE INFO

Article history:
Received 10 May 2011
Accepted 19 May 2011
Available online 27 May 2011

Keywords:
Counter-current chromatography
modelling
Stationary phase retention
Phase mixing
Helical column
Spiral column
Multi-layer column

ABSTRACT

Unlike the existing 2-D pseudo-ring model for helical columns undergoing synchronous type-J planetary motion of counter-current chromatograph (CCC), the 3-D "helix" model developed in this work shows that there is a second normal force (i.e. the binormal force) applied virtually in the axial direction of the helical column. This force alternates in the two opposite directions and intensifies phase mixing with increasing the helix angle. On the contrary, the 2-D spiral column operated on the same CCC device lacks this third-dimensional mixing force. The (principal) normal force quantified by this "helix" model has been the same as that by the pseudo-ring model. With $\beta > 0.25$, this normal centrifugal force has been one-directional and fluctuates cyclically. Different to the spiral column, this "helix" model shows that the centrifugal force (i.e. the hydrostatic force) does not contribute to stationary phase retention in the helical column. Between the popular helical columns and the emerging spiral columns for type-J synchronous CCC, this work has thus illustrated that the former is associated with better phase mixing yet poor retention for the stationary phase whereas the latter has potential for better retention for the stationary phase yet poor phase mixing. The methodology developed in this work may be regarded as a new platform for designing optimised CCC columns for analytical and engineering applications.

1. Introduction

The core specialist technology of a counter-current chromatography (CCC) system consists of device type and column geometry. For the device type (also termed as centrifuge scheme), the synchronous type-J CCC provides a better balance between application needs and marketing reality. The type-J CCC device has been extensively compared with the other types (e.g. cross-axis, type-I and non-synchronous) over the past 30 years. Interestingly, its importance has been strengthened rather than weakened as a result of these comparisons, with even increasing applications and device sizes [1–6]. For the column geometry, the multi-layer helical column (Fig. 1A) stood out from all the known types of column geometry (e.g. toroidal and spiral columns) early on [3,7–10]. Multilayer columns on type-J CCC devices have been most widely used not only in laboratory research and development, but also for preparative and in commercial large-scale production [5].

Against this background, it has been essential to comprehend the unique physical nature for two immiscible liquid phases contained in the multi-layer helical column undergoing a synchronous type-J planetary motion. Specifically, it needs to be understood how a liquid stationary phase is retained in the column, and how and to what extent periodical phase mixing and settling occur.

To explain the retention of a liquid stationary phase, a long-held belief has been that "all objects with different densities, either lighter or heavier than the suspending medium, present in the rotating coil are driven toward the head of the coil" [11]. This type of forces has vaguely been termed as the Archimedean screw force (effect) [12–14]. According to our more recent work, under the type-J planetary rotation and with $\beta > 0.5$, the internal surface of the column exerts a drag force (a hydrodynamic force) primarily in the head-to-tail (not tail-to-head) direction, irrespective of heavy or light phase. Nevertheless, that work showed that this drag force, to a large extent, applies to the heavy phase and to a less extent to the light phase (see Fig. 4 of Ref. [13]). This solid-to-liquid drag force (i.e. the Archimedean screw force) can be arranged to counteract the liquid-to-liquid drag force caused by flowing the mobile phase through the stationary phase, and consequently the liquid stationary phase could be retained throughout the tubular path of the column to a reasonable extent. In addition, the Archimedean screw force is monotonically related to the β-value for this device type, especially when $\beta \geq 0.5$ [13]. These findings have more correctly described the working of CCC for retaining a liquid stationary phase and can explain why stationary phase retention reduces with

* Corresponding author at: State Key Laboratory of Bioreactor Engineering, East China University of Science & Technology, Shanghai 200237, China.
Tel.: +86 (0)21 64253032; fax: +86 (0)21 64253702.
E-mail address: hugh.guan@hotmail.com (Y.H. Guan).

0021-9673/$ – see front matter © 2011 Elsevier B.V. All rights reserved.
doi:10.1016/j.chroma.2011.05.078

Nomenclature

$a_{\text{B-helix}}$	value of acceleration vector in binormal directions on the helical coil
$a_{\text{B-ring}}$	value of acceleration vector in binormal directions on the pseudo-ring coil
$a_{\text{B-spiral}}$	value of acceleration vector in binormal directions on the spiral coil
$\boldsymbol{a}_{\mathbf{helix}}$	acceleration vector for any location on the helical coil
$a_{\text{N-helix}}$	value of acceleration vector in normal directions on the helical coil
$a_{\text{N-ring}}$	value of acceleration vector in normal directions on the pseudo-ring coil
$a_{\text{N-spiral}}$	value of acceleration vector in normal directions on the spiral coil
$\boldsymbol{a}_{\mathbf{ring}}$	acceleration vector for any location on the pseudo-ring coil
$a_{\text{t-helix}}$	value of acceleration vector in tangential directions on the helical coil
$a_{\text{t-ring}}$	value of acceleration vector in tangential directions on the pseudo-ring coil
$a_{\text{t-spiral}}$	value of acceleration vector in tangential directions on the spiral coil
$\widehat{\boldsymbol{B}}_{\mathbf{helix}}$	unit binormal vector for any location on the helical coil
$\widehat{\boldsymbol{B}}_{\mathbf{ring}}$	unit binormal vector for any location on the pseudo-ring coil
$\boldsymbol{i}$	unit vector at the x-axis direction in the Cartesian coordinate system
$\boldsymbol{j}$	unit vector at the y-axis direction in the Cartesian coordinate system
$\boldsymbol{k}$	unit vector at the z-axis direction in the Cartesian coordinate system
$\widehat{\boldsymbol{N}}_{\mathbf{helix}}$	unit normal vector for any location on the helical coil
$\widehat{\boldsymbol{N}}_{\mathbf{ring}}$	unit normal vector for any location on the pseudo-ring coil
R	rotation radius of the rotor
$\boldsymbol{S}_{\mathbf{helix}}$	location vector for any location on the helical coil
$\boldsymbol{S}_{\mathbf{ring}}$	location vector for any location on the pseudo-ring coil
S_x	value of location vector at the x-axis direction in the Cartesian coordinate system
S_y	value of location vector at the y-axis direction in the Cartesian coordinate system
S_z	value of location vector at the z-axis direction in the Cartesian coordinate system
t	time
$\widehat{\boldsymbol{T}}_{\mathbf{helix}}$	unit tangential vector for any location on the helical coil
$\widehat{\boldsymbol{T}}_{\mathbf{ring}}$	unit tangential vector for any location on the pseudo-ring coil
$u_{\text{t-helix}}$	value of velocity vector in tangential directions on the helical coil
$u_{\text{t-ring}}$	value of velocity vector in tangential directions on the pseudo-ring coil
$u_{\text{t-spiral}}$	value of velocity vector in tangential directions on the spiral coil
$\boldsymbol{u}_{\mathbf{ring}}$	velocity vector for any location on the pseudo-ring coil
$\boldsymbol{u}_{\mathbf{helix}}$	velocity vector for any location on the helical coil
x	x-axis in the Cartesian coordinate system (see Fig. 2)
y	y-axis in the Cartesian coordinate system (see Fig. 2)
z	z-axis in the Cartesian coordinate system (see Fig. 2)
x'	x'-axis in the Cartesian coordinate system for the coil self-rotation (see Fig. 2)
y'	y'-axis in the Cartesian coordinate system for the coil self-rotation (see Fig. 2)
z'	z'-axis in the Cartesian coordinate system for the coil self-rotation (see Fig. 2)

Greek letters

α	helix angle of the helical coil with $0 < \alpha < \pi/2$
β	radius ratio of the bobbin self-rotation to the rotor rotation ($\beta = r/R$)
θ	elapsed rotation angle of the rotor ($\theta > 0$ for counter-clockwise rotation)
φ	angular location for any position on CCC coil
ω	rotational angular speed of the rotor where $\omega = d\theta/dt$

increasing mobile phase flow rate and often increases with increasing rotational speed of the rotor.

The locus of a type-J planetary motion is always and only two-dimensional. For synchronous type-J planetary motion (Fig. 2C), this is described by Ito [15] as,

$$\begin{cases} x = R\cos\theta + \beta R\cos(2\theta) \\ y = R\sin\theta + \beta R\sin(2\theta) \end{cases} \quad (1)$$

Whilst Eq. (1) has correctly described the locus of type-J synchronous planetary motion, an improved understanding for physical forces leading to stationary phase retention and the mixing-settling pattern of the two liquid phases requires the information on the column geometry. These effects can be understood by velocity and acceleration vectors in the tangential direction and directions normal to the tangential [13]. Notably, the velocity vector at the tangential direction can be used to describe the solid surface-to-liquid drag force (i.e. the Archimedean screw force) which is a characteristic force leading to stationary phase retention in the CCC column. The net acceleration vector at the tangential direction determines if hydrostatic centrifugal force contributes to the retention of stationary phase, whereas the acceleration vectors at directions normal to the tangential reflect the mixing-settling pattern of the liquid phases contained in the column.

By assuming the CCC column as a pseudo-ring coil, location vector on such a column undergoing the dynamic motion [i.e. Eq. (1)] can thus be quantified in the 3-D Cartesian coordinate system as,

$$\boldsymbol{S}_{\boldsymbol{ring}} = R[\cos\theta + \beta\cos(2\theta + \varphi)]\boldsymbol{i} + R[\sin\theta + \beta\sin(2\theta + \varphi)]\boldsymbol{j} + 0\boldsymbol{k} \quad (2)$$

In Eq. (2), the initial angle for location on the column, φ, is added into Eq. (1) to generalise the original model derived from Eq. (1). This generalization is necessary as it allows for distinguishing different locations on the coil. For the pseudo-ring model the physical property on each location is identical except for timing, but this is not the case for other types of coil geometry such as the spiral coil [13]. For the helical coil geometry the, introduction of this angular location allows for mathematical treatment on this coil geometry [e.g. Eqs. (9)–(11) below]. Of course, Eq. (1) can be regarded as being for the location described by Eq. (2) at $\varphi = 0$.

The "spiral" model developed for the spiral column (Fig. 1C) on a synchronous type-J device can be used to demonstrate the importance of such geometry [13]. This "spiral" model simplifies the spiral column into a portion of the two-dimensional, infinitely

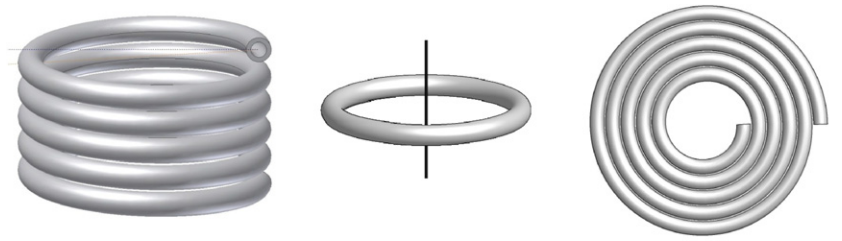

(A) A 3-dimentionla helical column (B) A tubular column to represent pseudo-ring column (C) A 2-dimensional spiral column

Fig. 1. An illustration of (A) the helical column, (B) the pseudo-ring column and (C) the spiral column studied in this work.

thin Archimedean spiral. Quantitative analyses showed that this column geometry on synchronous type-J CCC is associated with a net tangential centrifugal force along the spiral coil path (termed as the tangential centrifugal force) and this hydrostatic force can be arranged to contribute to stationary phase retention along with the Archimedean screw force [13,16]. This finding supported experimental observations that satisfactory stationary phase retention can hardly be achieved within multi-layer helical columns for aqueous polymer two-phase systems (ATPSs) [13,17,18] whereas this retention problem can be resolved with spiral columns on synchronous type-J CCC devices [4,16,19]. Even with this beneficial physical effect, however the acceleration vector at the normal direction does not show noticeably improvement on phase mixing intensities with the spiral column [20]. In the literature, this poor mixing situation has largely been attributed to the low mass transfer rate for large molecules such as proteins [4]. Of course, one could argue for the same mass transfer problem for helical columns, but a conceivable defence might be that such data are not available for helical columns due presumably to the low stationary phase retention for this type of columns. Interestingly, our results in the present paper will show that phase mixing in the spiral column is likely to be worse off as compared with the helical column.

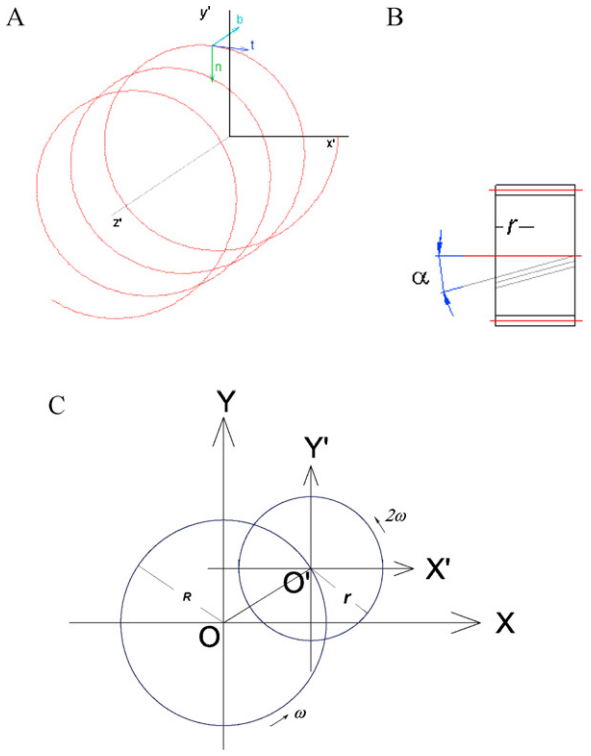

Fig. 2. An illustration of the "helix" model. (A) 3-D illustration in x'–y'–z Cartesian coordinate system for tangential, normal and binormal vectors, (B) illustration for helix angle (α) on the helical coil, and (C) illustration for the rotation of the rotor on the x–y Cartesian coordinate system and the self-rotation of the coil on the x'–y' Cartesian coordinate system with type-J synchronous planetary motion.

Over the past three decades the most popular 3-D multilayer helical column has been consistently modelled as an infinitely thin, closed 2-D pseudo ring (see Fig. 1B for such an imaginary circular column). With such a simplified geometry, normal and radial vectors are identical. The unit vectors for such geometry at tangential, normal and binormal directions can be summarised as,

$$\widehat{\boldsymbol{T}}_{\text{ring}} = -\sin(2\theta+\varphi)\boldsymbol{i} + \cos(2\theta+\varphi)\boldsymbol{j} + 0\boldsymbol{k} \tag{3A}$$

$$\widehat{\boldsymbol{N}}_{\mathbf{ring}} = -\cos(2\theta+\varphi)\boldsymbol{i} - \sin(2\theta+\varphi)\boldsymbol{j} + 0\boldsymbol{k} \tag{3B}$$

$$\widehat{\boldsymbol{B}}_{\mathbf{ring}} = 0\boldsymbol{i} + 0\boldsymbol{j} + \boldsymbol{k} \tag{3C}$$

By all means, Eqs. (3A)–(3C) can be derived using Eqs. (9)–(11). Using the geometric information expressed in Eqs. (3A)–(3C), the relevant vectors for the pseudo-ring model in the 3-D Cartesian coordinate system can be expressed as (see also Ref. [21]),

$$\boldsymbol{u}_{\mathbf{ring}} = \left[\frac{\partial \boldsymbol{S}_{\mathbf{ring}}}{\partial\theta}\right]_{\beta,\varphi}\cdot\frac{d\theta}{dt} = -\omega R[\sin\theta + 2\beta\sin(2\theta+\varphi)]\boldsymbol{i} + \omega R[\cos\theta + 2\beta\cos(2\theta+\varphi)]\boldsymbol{j} + 0\boldsymbol{k} \tag{4}$$

$$\boldsymbol{a}_{\mathbf{ring}} = \left[\frac{\partial^2 \boldsymbol{S}_{\mathbf{ring}}}{\partial\theta^2}\right]_{\beta,\varphi}\cdot\left(\frac{d\theta}{dt}\right)^2 = -\omega^2 R[\cos\theta + 4\beta\cos(2\theta+\varphi)]\boldsymbol{i} - \omega^2 R[\sin\theta + 4\beta\sin(2\theta+\varphi)]\boldsymbol{j} + 0\boldsymbol{k} \tag{5}$$

The corresponding vectors at the tangential, normal and binomial directions for the pseudo-ring model can be obtained as,

$$\boldsymbol{u}_{\mathbf{ring}} = (\boldsymbol{u}_{\mathbf{ring}}\cdot\widehat{\boldsymbol{T}}_{\mathbf{ring}})\widehat{\boldsymbol{T}}_{\mathbf{ring}} + (\boldsymbol{u}_{\mathbf{ring}}\cdot\widehat{\boldsymbol{N}}_{\mathbf{ring}})\widehat{\boldsymbol{N}}_{\mathbf{ring}} + (\boldsymbol{u}_{\mathbf{ring}}\cdot\widehat{\boldsymbol{B}}_{\mathbf{ring}})\widehat{\boldsymbol{B}}_{\mathbf{ring}} = \omega R[\cos(\theta+\varphi) + 2\beta]\widehat{\boldsymbol{T}}_{\mathbf{ring}} - \omega R\sin(\theta+\varphi)\widehat{\boldsymbol{N}}_{\mathbf{ring}} + 0\widehat{\boldsymbol{B}}_{\mathbf{ring}} \tag{6}$$

$$\boldsymbol{a}_{\mathbf{ring}} = (\boldsymbol{a}_{\mathbf{ring}}\cdot\widehat{\boldsymbol{T}}_{\mathbf{ring}})\widehat{\boldsymbol{T}}_{\mathbf{ring}} + (\boldsymbol{a}_{\mathbf{ring}}\cdot\widehat{\boldsymbol{N}}_{\mathbf{ring}})\widehat{\boldsymbol{N}}_{\mathbf{ring}} + (\boldsymbol{a}_{\mathbf{ring}}\cdot\widehat{\boldsymbol{B}}_{\mathbf{ring}})\widehat{\boldsymbol{B}}_{\mathbf{ring}} = \omega^2 R\sin(\theta+\varphi)\widehat{\boldsymbol{T}}_{\mathbf{ring}} + \omega^2 R[\cos(\theta+\varphi) + 4\beta]\widehat{\boldsymbol{N}}_{\mathbf{ring}} + 0\widehat{\boldsymbol{B}}_{\mathbf{ring}} \tag{7}$$

On the one hand, this pseudo-ring model has successfully explained the effects of the rotor's rotation speed (ω) and the β value on stationary phase retention and phase mixing intensities. On the other hand, the pseudo-ring model simplifies the 3-D helical geometry into a 2-D planetary geometry, and so cannot shed any

light on the effect of the helix angle on the performance on type-J CCC in applications typically in chromatographic separations. Given that an essential feature of the CCC column is to possess both "head" and "tail" terminals, such a "ring" model should be regarded as being physically oversimplified. The aim of the present work is to model the multi-layer helical column as a three-dimensional, infinitely thin and single layer 3-D helix (hence termed as "helix" model) and to quantitatively compare the helical column with the pseudo-ring column and the spiral column for physical forces determining the working of CCC.

2. Establishment of the "helix" model for the helical column undergoing type-J synchronous planetary motion

The column geometry is simplified as a curve in the 3-D Cartesian coordinate (see Fig. 2). By introducing the helix angle (α), the location vector for the left-handed helical coil can be resolved as,

$$\boldsymbol{S}_{\mathbf{helix}} = S_x\boldsymbol{i} + S_y\boldsymbol{j} + S_z\boldsymbol{k} = [R\cos\theta + \beta R\cos(2\theta+\varphi)]\boldsymbol{i} + [R\sin\theta + \beta R\sin(2\theta+\varphi)]\boldsymbol{j} + (2\theta+\varphi)\beta R\cdot\tan(\alpha)\boldsymbol{k} \quad (8)$$

Unit tangential vector ($\widehat{\boldsymbol{T}}_{\mathbf{helix}}$), unit normal vector ($\widehat{\boldsymbol{N}}_{\mathbf{helix}}$) and unit binormal vector ($\widehat{\boldsymbol{B}}_{\mathbf{helix}}$) for the helical coil geometry are obtained as follows,

$$\widehat{\boldsymbol{T}}_{\mathbf{helix}} = \frac{\partial \boldsymbol{S}_{\mathbf{helix}}}{\partial\varphi}\cdot\left|\frac{\partial \boldsymbol{S}_{\mathbf{helix}}}{\partial\varphi}\right|^{-1} = \frac{1}{\sqrt{1+\tan^2(\alpha)}}[-\sin(2\theta+\varphi)\boldsymbol{i} + \cos(2\theta+\varphi)\boldsymbol{j} - \tan(\alpha)\boldsymbol{k}] \quad (9)$$

$$\widehat{\boldsymbol{N}}_{\mathbf{helix}} = \frac{\partial \boldsymbol{T}_{\mathbf{helix}}}{\partial\varphi}\cdot\left|\frac{\partial \boldsymbol{T}_{\mathbf{helix}}}{\partial\varphi}\right|^{-1} = --\cos(2\theta+\varphi)\boldsymbol{i} - \sin(2\theta+\varphi)\boldsymbol{j} + 0\boldsymbol{k} \quad (10)$$

$$\widehat{\boldsymbol{B}}_{\mathbf{helix}} = \frac{\widehat{\boldsymbol{T}}_{\mathbf{helix}}\times\widehat{\boldsymbol{N}}_{\mathbf{helix}}}{\left|\widehat{\boldsymbol{T}}_{\mathbf{helix}}\times\widehat{\boldsymbol{N}}_{\mathbf{helix}}\right|} = \frac{\tan(\alpha)}{\sqrt{1+\tan^2(\alpha)}}\left[\sin(2\theta+\varphi)\boldsymbol{i} + \cos(2\theta+\varphi)\boldsymbol{j} + \frac{1}{\tan(\alpha)}\boldsymbol{k}\right] \quad (11)$$

Each point on the helical coil undergoes type-J synchronous planetary motion, and so its velocity and acceleration vectors are the same as those inherent to the pseudo-ring model on the x–y–z Cartesian coordinate system, as quantified by Eqs. (4) and (5). As such, the respective vectors at the tangential, normal and binormal directions for any points on the helical coil undergoing the synchronous type-J planetary motion can be obtained as follows.

$$\boldsymbol{u}_{\mathbf{helix}} = (\boldsymbol{u}_{\mathbf{ring}}\cdot\widehat{\boldsymbol{T}}_{\mathbf{helix}})\widehat{\boldsymbol{T}}_{\mathbf{helix}} + (\boldsymbol{u}_{\mathbf{ring}}\cdot\widehat{\boldsymbol{N}}_{\mathbf{helix}})\widehat{\boldsymbol{N}}_{\mathbf{helix}} + (\boldsymbol{u}_{\mathbf{ring}}\cdot\widehat{\boldsymbol{B}}_{\mathbf{helix}})\widehat{\boldsymbol{B}}_{\mathbf{helix}} = \frac{\omega R[\cos(\theta+\varphi)+2\beta]}{\sqrt{1+\tan^2(\alpha)}}\widehat{\boldsymbol{T}}_{\mathbf{helix}} - \omega R\sin(\theta+\varphi)\widehat{\boldsymbol{N}}_{\mathbf{helix}} + \frac{\omega R\cdot\tan(\alpha)[\cos(3\theta+\varphi)+2\beta\cdot\cos(4\theta+2\varphi)]}{\sqrt{1+\tan^2(\alpha)}}\widehat{\boldsymbol{B}}_{\mathbf{helix}} \quad (12)$$

and

$$\boldsymbol{a}_{\mathbf{helix}} = (\boldsymbol{a}_{\mathbf{ring}}\cdot\widehat{\boldsymbol{T}}_{\mathbf{helix}})\widehat{\boldsymbol{T}}_{\mathbf{helix}} + (\boldsymbol{a}_{\mathbf{ring}}\cdot\widehat{\boldsymbol{N}}_{\mathbf{helix}})\widehat{\boldsymbol{N}}_{\mathbf{helix}} + (\boldsymbol{a}_{\mathbf{ring}}\cdot\widehat{\boldsymbol{B}}_{\mathbf{helix}})\widehat{\boldsymbol{B}}_{\mathbf{helix}} = \frac{\omega^2 R\cdot\sin(\theta+\varphi)}{\sqrt{1+\tan^2(\alpha)}}\widehat{\boldsymbol{T}}_{\mathbf{helix}} + \omega^2 R[\cos(\theta+\varphi)+4\beta]\widehat{\boldsymbol{N}}_{\mathbf{helix}} - \frac{\omega^2 R\cdot\tan(\alpha)\sin(\theta+\varphi)}{\sqrt{1+\tan^2(\alpha)}}\widehat{\boldsymbol{B}}_{\mathbf{helix}} \quad (13)$$

3. Results and discussion

For any types of CCC columns, the level of stationary phase retention is determined by the Archimedean screw force (i.e. the hydrodynamic force) and the tangential centrifugal force (i.e. the hydrostatic force for high-speed CCC) (if any). The Archimedean screw force is represented by the tangential velocity vector [13,14] and these are shown in Eqs. (14)–(16) for the pseudo-ring column, the helical column and the spiral column respectively (Table 1). The tangential centrifugal forces for the pseudo-ring column, the helical column and the spiral column are described in Eqs. (17)–(19) respectively (Table 1).

The phase mixing pattern and intensity within any CCC columns can be quantified by the two centrifugal forces perpendicular to the tangential direction of the coil path. These are the (principal) normal centrifugal force and the binormal centrifugal force. The (principal) normal force is located on the flat pseudo-ring plain, the flat spiral coil plain, or in the similar directions for the helical coil. These are described in Eqs. (20)–(22) respectively for the pseudo-ring column, the helical column and the spiral column (Table 1). The binormal centrifugal force is almost perpendicular to the pseudo-ring, to the spiral plain, or approximately in the axial direction of the helical column (see Fig. 2A). The binormal centrifugal force is described by Eqs. (23)–(25) for the pseudo-ring column, the helical column and the spiral column respectively (Table 1), but except for the helical column their values are invariably zero.

Between the three models, the "helix" model can be degenerated to the pseudo-ring model when the helix angle $\alpha = 0$. This is so from $u_{\text{t-helix}}$ [Eq. (15)] to $u_{\text{t-ring}}$ [Eq. (14)], from $a_{\text{t-helix}}$ [Eq. (18)] to $a_{\text{t-ring}}$ [Eq. (17)], and from $a_{\text{B-helix}}$ [Eq. (24)] to $a_{\text{B-ring}}$ [Eq. (23)] (all the equations are in Table 1). The "spiral" model merges with the pseudo-ring model at $\varphi\to\infty$. This is evident from $u_{\text{t-spiral}}$ [Eq. (16)] to $u_{\text{t-ring}}$ [Eq. (14)], from $a_{\text{t-spiral}}$ [Eq. (19)] to $a_{\text{t-ring}}$ [Eq. (17)], and from $a_{\text{N-spiral}}$ [Eq. (22)] to $a_{\text{N-ring}}$ [Eq. (20)] (all the equations are in Table 1).

3.1. Centrifugal force does not contribute to stationary phase retention in 3-D helical columns

In the tangential direction of a column path, the stationary phase is subjected to net balanced (either hydrostatic or hydrodynamic) physical forces, the interplay of which determines the level of stationary phase retention. As was previously verified [13,14,21] and is shown in Eq. (17) of Table 1, the net tangential centrifugal force (i.e. the hydrostatic force) for the pseudo-ring column in high speed CCC fluctuates cyclically and its net value over each rotation of the rotor is always zero. Eq. (18) of Table 1 shows that there is no net hydrostatic force at tangential directions for the helical column as well. Clearly, the centrifugal force does not contribute to stationary phase retention for both the pseudo-ring column and the helical column. This result has been different to the popular opinion in this research area as there has been a vague understanding that centrifugal force causes the unusual stationary phase retention in the CCC columns. Perhaps there has been confusion between the hydrostatic centrifugal force and the hydrodynamic Archimedean screw force among the practitioners of the CCC technology. Indeed, the more correct

Table 1
A list of equations for describing stationary phase retention and phase mixing within the pseudo-ring column, the helical column and the spiral column undergoing type-J synchronous planetary motion of counter-current chromatography.

(1) The Archimedean screw force (the hydrodynamic force)		
The pseudo-ring column	$u_{\text{t-ring}} = \omega R[\cos(\theta+\varphi)+2\beta]$	(14)
The helical column	$u_{\text{t-helix}} = \dfrac{\omega R}{\sqrt{1+\tan^2(\alpha)}}[\cos(\theta+\varphi)+2\beta]$	(15)
The spiral column	$u_{\text{t-spiral}} = \omega R\dfrac{\varphi}{\sqrt{1+\varphi^2}}\left[\cos(\theta+\varphi)+2\beta+\dfrac{\sin(\theta+\varphi)}{\varphi}\right]$	(16)
(2) The tangential centrifugal force (the primary hydrostatic force)		
The pseudo-ring column	$a_{\text{t-ring}} = \omega^2 R\cdot\sin(\theta+\varphi)$	(17)
The helical column	$a_{\text{t-helix}} = \dfrac{\omega^2 R}{\sqrt{1+\tan^2(\alpha)}}\cdot\sin(\theta+\varphi)$	(18)
The spiral column	$a_{\text{t-spiral}} = \omega^2 R\dfrac{\varphi}{\sqrt{1+\varphi^2}}\cdot\left[\sin(\theta+\varphi)-\dfrac{\cos(\theta+\varphi)+4\beta}{\varphi}\right]$	(19)
(3) The normal centrifugal force (the primary hydrostatic force)		
The pseudo-ring column	$a_{\text{N-ring}} = \omega^2 R[\cos(\theta+\varphi)+4\beta]$	(20)
The helical column	$a_{\text{N-helix}} = \omega^2 R[\cos(\theta+\varphi)+4\beta]$	(21)
The spiral column:	$a_{\text{N-spiral}} = \omega^2 R\dfrac{\varphi}{\sqrt{4+\varphi^2}}\left[\cos(\theta+\varphi)+4\beta+\dfrac{2\sin(\theta+\varphi)}{\varphi}\right]$	(22)
(4) The binormal centrifugal force (the primary hydrostatic force which is exactly or approximately perpendicular to the flat "ring")		
The pseudo-ring column	$a_{\text{B-ring}} = 0$	(23)
The helical column	$a_{\text{B-helix}} = -\dfrac{\omega^2 R\cdot\tan(\alpha)}{\sqrt{1+\tan^2(\alpha)}}\sin(\theta+\varphi)$	(24)
The spiral column	$a_{\text{B-spiral}} = 0$	(25)

role for the tangential centrifugal force in contributing to stationary phase retention was unravelled only recently [13,14].

An increase of the helix angle reduces the amplitude of this tangential waving force for helical columns. Theoretically, this could slightly lessen the swish-swash movement for the stationary phase in the column and could somewhat worsen phase mixing in the (principal) normal direction. With a low helix angle, it is almost certain that the 'ring' and the 'helix' models are inter-replaceable in describing the tangential centrifugal force [i.e. Eqs. (17) and (18) of Table 1].

3.2. The effect of the helix angle on stationary phase retention

As has been well understood, stationary phase retention can be improved by increasing the Archimedean screw force (the primary hydrodynamic force) [13,14], which is described by the tangential velocity for the helical coil Eq. (15) and that for the pseudo-ring coil Eq. (14) (in Table 1). Both Eqs. (14) and (15) of Table 1 indicate that an increase of the rotation speed for the rotor or that of the β value monotonically augment the Archimedean screw force and hence would improve the stationary phase retention. Eq. (15) of Table 1 shows that, with $\beta > 0.5$ an increase of the helix angle reduces the Archimedean screw force, and this effect can become more detectable when the helix angle α becomes large.

3.3. The effect of the helix angle on phase mixing

The phase mixing intensity and pattern are determined by the (principal) normal acceleration vector and the binormal acceleration vector. Eqs. (20) and (21) of Table 1 show that the normal acceleration vectors for the pseudo-ring column and the helical column are identical. With $\beta > 0.25$, this normal force does not alter directions but alter its magnitude. Consequently, the mixing intensity for the phases would have been weak and only wavelike mixing would prevail [16,22,23].

However, the binormal acceleration vector for the helical column [i.e. Eq. (24) of Table 1] is completely different to that for the pseudo-ring column [i.e. Eq. (23) of Table 1]. The helical column registers a cyclical force normal to both the tangential direction and the (principal) normal direction, which is approximately in the axial direction of a helical column. For the pseudo-ring column, there is simply no such a force in that direction. Undoubtedly, this binormal force can improve phase mixing in the axial direction of the helical column. Fig. 3(A) compares this binormal acceleration force for small helix angles at 1.09°, 1.64° and 2.19° (with an equal increment of 0.55°) along with the normal acceleration force, whereas Fig. 3(B) makes similar comparisons for large helix angles at 15°, 30° and 45° (with an equal increment of 15°) respectively. With the increase of helix angle, this alternating binormal force (roughly in the axial direction of a helical column) becomes intensified. It is obvious that high helix angles can cause high levels of mixing intensity in the axial direction of a helical coil.

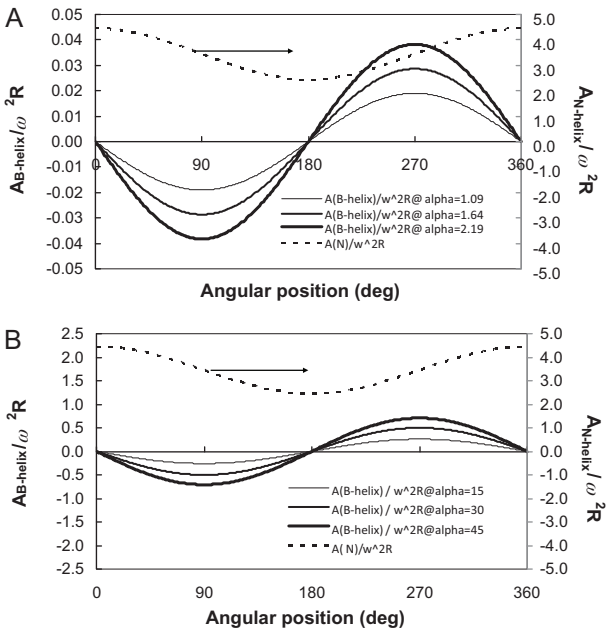

Fig. 3. Influence of helix angle on binormal centrifugal force of the helical column under the column/device parameter $\beta = 0.863$, $\theta = 0$. The normal centrifugal force is also plotted to show that it is not affected by the change of helix angle. (A) Helix angle at 1.09°, 1.64° and 2.19°. (B) Helix angle at 15°, 30° and 45°.

3.4. Comparison between the helical and the spiral columns

Using the theoretical framework established in the present and the previous work [13], it is possible to compare stationary phase retention and phase mixing between the spiral and helical columns. The equations for comparing these two types of column geometries are paired as Eqs. (15) and (16), Eqs. (18) and (19), Eqs. (21) and (22), and Eqs. (24) and (25) in Table 1.

3.4.1. Stationary phase retention

Both the Archimedean screw force (the hydrodynamic force) and the tangential centrifugal force (the primary hydrostatic force) can contribute to the stationary phase retention in a CCC column. When $\beta > 0.5$ the tangential velocity vector for the helical column invariably points to the self-rotation direction of the helical coil [Eq. (15) in Table 1] and shows the presence of net hydrodynamic force (i.e. the Archimedean screw force) for retaining the stationary phase in that direction.

The corresponding Archimedean screw force for the spiral column [described by Eq. (16)] is virtually the same as that for the helical column [described by Eq. (15) in Table 1]. This statement is demonstrated by the following calculation. In order to compare the tangential velocity magnitude in a like-to-like footing between the helical column and the spiral column, β value of the spiral coil is fixed at the same value as its helical coil counterpart. In this paper, a high value of $\beta = 0.863$ was artificially used for the helical coil. The Archimedean constant for the spiral coil was chosen as $k = 0.1$ cm and $R = 10$ cm (see Refs. [13,16] for such a spiral column). At $\beta = 0.863$, the corresponding angular location was calculated as $\varphi = 86.3$ rad (or 4947°). For this pair of locations in the two column geometries with the helix angle $\alpha = 0$, the ratio between the two tangential velocities $u_{\text{T-spiral}}/u_{\text{T-helix}} = 0.99$. Of course, Eq. (15) in Table 1 shows that the Archimedean screw force for the helix angle becomes weak as the helix angle increases.

Eq. (18) in Table 1 shows that the net tangential centrifugal force for the helical column is invariably zero. For the spiral column, the tangential centrifugal force [described by Eq. (19) in Table 1] can point to one direction for a range of locations, and so its net value becomes one-directional [13].

Both the tangential centrifugal force and the Archimedean screw force for the spiral column can be arranged to work in the same direction so that stationary phase retention can be considerably improved with this type of column geometry. This theoretical result can be consistently supported by experimental results using spiral columns for ATPSs [4,16,19]. On the other hand, the stationary phase retention for the helical column cannot in anyway rely on the tangential centrifugal force, but is determined solely by the magnitude of Archimedean screw force and the intensity of this is weakened with increasing the helix angle.

Overall, the spiral column possesses properties for achieving good stationary phase retention for polar phase systems such as ATPSs, whereas the helical column tends to be deficient in retaining a satisfactory level of stationary phase especially when the helix angle becomes large.

3.4.2. Phase mixing pattern and intensity

The spiral column possesses the normal centrifugal force in the spiral plain [as shown by Eq. (22) in Table 1] which is perpendicular to the tangential direction whereas there is no force causing phase mixing in the direction perpendicular to the spiral plain [as shown by Eq. (25) in Table 1]. The helical column is associated with two orthogonal mixing forces [i.e. the normal centrifugal force shown in Eq. (21) of Table 1] and the binormal centrifugal force shown in Eq. (24) of Table 1]. With $\beta > 0.25$, the normal centrifugal force for the helical column is invariably in one direction [Eq. (21) in Table 1]. Consequently, phase mixing occurs wavelike at the interphase and hence is low efficient. In order to compare the normal hydrostatic force in a like-to-like footing between the helical column and the spiral column, again β value of the spiral coil is fixed at the same value as for the helical column (see Section 3.4.1 above). As a demonstration, a high value of $\beta = 0.863$ was used for the two coil geometries. The Archimedean constant for the spiral coil was chosen as being $k = 0.1$ cm and $R = 10$ cm (see Refs. [13,16] for such a spiral CCC column). The corresponding angular location for the spiral coil was obtained from Eq. (22) of Table 1 as $\varphi = 86.3$ rad (or 4947°). For this pair of comparable locations for the two column geometries, the ratio between the two normal centrifugal forces $a_{\text{N-spiral}}/a_{\text{N-helix}} = 0.99$. The indication thus is that, for small helix angle, the phase mixing pattern and intensity between the helical column and the spiral column in the normal direction are virtually the same.

The second orthogonal mixing force for the helical column is approximately in the axial direction of a helical coil. As shown in Eq. (24) of Table 1, this alternating mixing force is intensified with the increase of helix angle. Of course, there is no mixing tendency in the binormal directions for the spiral coil.

Compared to the spiral column, the helical column possesses an additional dimension of alternating phase mixing force and the mixing intensity of this force increases with increasing the helix angle.

3.4.3. Dilemma between the helical column and the spiral column

The helical column undergoing type-J synchronous planetary motion has a propensity for achieving better phase mixing inside the column, but suffers from the property associated with poor stationary phase retention. On the contrary, the spiral column has the possibility for reaching satisfactory stationary phase retention, but suffers from the tendency associated with less satisfactory level of phase mixing.

These theoretical results can now be supported by a myriad of experimental evidences in the literature (see, e.g. Table 1 of Ref. [18] for an experimentally based summary). For instance, technological successes for multi-layer helical columns have been solely for those easy-to-retain aqueous-organic two-phase phase systems, rather than for difficult-to-retain systems such as ATPSs. To overcome the inherent restriction of helical columns on stationary phase retention, spiral columns have been developed for considerably improving stationary phase retention of ATPSs for dealing with large molecules and/or nano-particles. With a sound theoretical basis, the present work shows clearly that such an improvement in stationary phase retention using spiral columns has been at the cost of complete loss of alternating phase mixing tendency in the near axial direction of helical columns. It is therefore not surprising that efforts have been made to recover the loss of phase mixing tendency in spiral columns and a more successful measure was the construction of barricaded spiral channels for improving phase mixing [20].

4. Conclusions

Based on the existing 2-D models for CCC columns, we have established the 3-D physical model for the helical column (termed as the helix model) undergoing type-J synchronous planetary motion, and have used this model to understand the effect of helix angle on the phase behaviour for the most popular multi-layer helical column geometry.

It can be concluded that this 3-D helix model entails important information that the existing 2-D pseudo-ring model lacks. Com-

pared with the use of the presently popular 2-D pseudo-ring model for helical columns, the advantages for using this 3-D helix model are not just at a quantitative level, but more importantly at the qualitative level.

This work may have opened a new avenue for designing new CCC columns before committing to time-consuming, expensive and more experience-orientated experimental adventures. Furthermore, the methodology demonstrated in this work can be supplementary to experimental explorations for new column designs on Type-J CCC devices (see Refs. [24,25] for a series of such efforts made recently). Based on known physical models for nearly all the types of CCC devices, the methodology pioneered in our group can be extended to other types of centrifuge devices operated either synchronously or non-synchronously. We have now been put in a sound theoretical footing to confidently address seemingly difficult yet pragmatic questions such as "what might be the gains for using cross-axis coil planet centrifuge as compared to type-J planetary motion?" and "are there "ideal" column geometries for a CCC device type?".

Acknowledgements

YHG acknowledges support by BBSRC Grants, BB/C5063341/1 and BB/FOF/206, and by KH Education & Technology. He is indebted to Ian Sutherland, Mike Brown, Derek Fisher and Hao Gao for their contributions, discussion or comments. The authors are most grateful to Dr. Y. Ito for carefully checking the manuscript and for pointing out experimental evidences to support the results obtained in this work.

References

[1] Y. Ito, CRC Rev. Anal. Chem. 17 (1986) 65.
[2] K. Shinomiya, J.-M. Menet, H.M. Fales, Y. Ito, J. Chromatogr. 644 (1993) 215.
[3] Y.H. Guan, D. Fisher, I.A. Sutherland, J. Chromatogr. A 1217 (2010) 3525.
[4] Y. Ito, Chem. Eng. Process. 49 (2010) 782.
[5] I. Sutherland, P. Hewitson, S. Ignatova, J. Chromatogr. A 1216 (2009) 4201.
[6] K. Shinomiya, Y. Kabasawa, K. Yanagidaira, H. Sasaki, M. Muto, T. Okada, Y. Ito, J. Chromatogr. A 1005 (2003) 103.
[7] K. Shinomiya, Y. Kabasawa, Y. Ito, J. Liq. Chromatogr. Relat. Technol. 21 (1998) 111.
[8] A. Degenhardt, M. Schwarz, P. Winterhalter, Y. Ito, J. Chromatogr. A 922 (2001) 355.
[9] J.L. Sandlin, Y. Ito, J. Liq. Chromatogr. 11 (1988) 55.
[10] Y. Ito, J. Chromatogr. 192 (1980) 75.
[11] Y. Ito, J. Chromatogr. A 1065 (2005) 145.
[12] Y. Ito, J. Liq. Chromatogr. 15 (1992) 2639.
[13] Y.H. Guan, D. Fisher, I.A. Sutherland, J. Chromatogr. A 1151 (2007) 136.
[14] P.L. Wood, J. Chromatogr. A 1217 (2010) 1283.
[15] Y. Ito, J. Chromatogr. 188 (1980) 33.
[16] Y.H. Guan, J. Smulders, D. Fisher, I.A. Sutherland, J. Chromatogr. A 1151 (2007) 115.
[17] A. Weisz, Y. Ito, J. Chromatogr. A, in press, doi:10.1016/j.chroma.2010.12.034.
[18] Y.H. Guan, E.C. Bourton, P. Hewitson, I.A. Sutherland, D. Fisher, Sep. Pur. Technol. 65 (2009) 79.
[19] X. Cao, G. Hu, L. Huo, X. Zhu, T. Li, J. Powell, Y. Ito, J. Chromatogr. A 1188 (2008) 164.
[20] Y. Ito, L. Qi, J. Powell, H. Sharpnack, H. Metger, J. Yost, X.-L. Cao, Y.-M. Dong, L.S. Huo, X. Zhu, T. Li, J. Chromatogr. A 1151 (2007) 108.
[21] J.-M. Menet, Y. Ito, J. Chromatogr. 644 (1993) 231.
[22] W.D. Conway, Countercurrent Chromatography: Apparatus, Theory, and Applications, VCH, Cambridge, 1990 (Chapter 5).
[23] I.A. Sutherland, J. Mutyjens, M. Prins, P. Wood, J. Liq. Chromatogr. Relat. Technol. 16 (2000) 2259.
[24] Y. Yang, D. Gu, H.A. Aisa, Y. Ito, J. Liq. Chromatogr. Relat. Technol. 33 (2010) 1542.
[25] Y. Ito, Z. Ma, R. Clary, J. Powell, M. Knight, T.M. Finn, J. Chromatogr. A, in press, doi:10.1016/j.chroma.2010.10.058.